

Lagrangian measurement of fluid-particle motion in an isotropic turbulent field

By YUKINARI SATO† AND KAZUO YAMAMOTO‡

Department of Chemical Engineering, Yokohama National University, Yokohama 240, Japan

(Received 21 February 1986)

By means of an optical tracer-particle tracking method, measurements for Lagrangian characteristics of turbulence, including the mean-square value of lateral diffusion from a point source $\overline{Y^2}$, the r.m.s. value of fluctuating velocity v' , the velocity autocorrelation coefficient $R_L(\tau)$, and the integral scale A_L , were made in approximately isotropic turbulent flow behind a grid. Comparison of these Lagrangian data with the Eulerian integral scale A_f and the double velocity correlation coefficient $f(r)$ led to the following results: (i) for a moderate turbulent Reynolds-number range of $Re_\lambda = 20$ – 70 , the ratio $\beta (= A_L/A_f)$ is within the values of 0.6–0.3, becoming lower as Re_λ increases, and (ii) the distribution of R_L against time lag τ is analogous to that of f against $\beta r/v'$. Further, it was confirmed by both theoretical analysis and experiments that the growth of $\overline{Y^2}(t)$ was weakened by the decay of turbulent energy, particularly so for long diffusion times.

1. Introduction

In discussing the mixing and diffusion of fluid in a turbulent flow, Taylor's turbulent diffusion theory (Taylor 1921; Hinze 1975), known as 'one-particle analysis', is often quoted, and many both theoretical and experimental aspects of this have been investigated. When investigating the diffusion of fluid elements, i.e. 'fluid particles', which is usually dealt with in an Eulerian framework, Lagrangian statistical characteristics such as the Lagrangian velocity autocorrelation play a very important role. Several theoretical approaches have therefore been proposed for determining the Lagrangian characteristics either directly or starting from their relationship to the Eulerian statistical characteristics of the random field. The most notable work among them may be the *independence approximation*, known as 'Corrsin's conjecture' proposed by Corrsin (1959). The independence approximation was used to explore the relationship between the Lagrangian autocorrelation and the Eulerian correlation by Saffman (1962), and its validity was confirmed theoretically by Weinstock (1976). Meanwhile, a numerical simulation of the Lagrangian autocorrelation was made by Kraichnan (1970). Hence it was possible to estimate whether the Lagrangian timescale is greater than, less than or equal to the Eulerian timescale. However, experimental data on the Lagrangian characteristics such as the mixing length, the Lagrangian velocity autocorrelation, etc. are too sparse and inaccurate to verify these approximations because of the absence of reliable methods for measuring the Lagrangian statistical characteristics of turbulence.

† Present address: R & D division, Nihon Kagaku Kogyo Co. Ltd, 2-1, Shimizu, Suita, Osaka 565, Japan.

‡ Present address: 719, Shin-maruko, Nakahara-ku, Kawasaki 211, Japan.

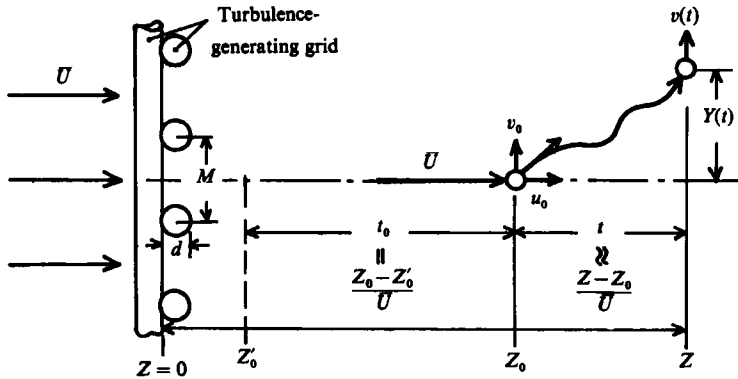


FIGURE 1. Particle displacement in grid turbulence.

In this study a measuring system has been developed for the acquisition of data on accurate Lagrangian statistical characteristics such as the velocity autocorrelation, based on the principle of an optical tracer-particle tracking method. The tracer particle used was sufficiently small to be almost without a buoyancy effect and so could be approximately regarded as a 'fluid particle'. This paper describes the measuring system and presents the experimental results for the Lagrangian properties of a flow in a nearly homogeneous and isotropic turbulent field behind a grid; these are quantitatively compared with Eulerian results in taking account of the decay of turbulence.

2. Theoretical relations

2.1. Fundamental equations for isotropic turbulence

According to Taylor's turbulent diffusion theory (1921), the lateral diffusion of fluid particles at time elapsed t due to fluctuation velocities v for homogeneous isotropic turbulence is expressed as a mean-square value $\overline{Y^2}$, as follows (see figure 1):

$$\overline{Y^2}(t) = 2 \int_0^t \int_0^{t'} \overline{v(t')v(t'-\tau)} d\tau dt'. \tag{1}$$

The Lagrangian velocity autocorrelation coefficient $R_L(\tau)$ for time lag τ is defined by

$$R_L(\tau) = \frac{\overline{v(t)v(t-\tau)}}{v'(t)v'(t-\tau)}, \tag{2}$$

where v' is the r.m.s. value of Lagrangian fluctuation velocity v , and the overbar denotes the ensemble-averaged value for a large number of fluid particles. Strictly, R_L should also be expressed as a function of time t as well as τ , but t is usually omitted in (2) because of the approximately steady treatment. Expressing the mean-square lateral diffusion $\overline{Y^2}$ and the turbulent diffusion coefficient \mathcal{D}_t using $R_L(\tau)$, we have

$$\overline{Y^2}(t) = 2 \int_0^t v'(t') \int_0^{t'} v'(t'-\tau) R_L(\tau) d\tau dt', \tag{3}$$

and

$$\mathcal{D}_t(t) = \frac{1}{2} \frac{d\overline{Y^2}}{dt} = v'(t) \int_0^t v'(t-\tau) R_L(\tau) d\tau. \tag{4}$$

2.2. Turbulent diffusion in a non-decaying energy field

In a homogeneous steady flow field where the decay of turbulent energy can be neglected, i.e. $v'(t) = v'(t-\tau) = v'$, the following equations for the diffusion process from a fixed point source are derived from (3) and (4):

$$\overline{Y^2}(t) = 2v'^2 \int_0^t \int_0^{t'} R_L(\tau) d\tau dt', \quad (5)$$

$$\mathcal{D}_t(t) = \frac{1}{2} \frac{d\overline{Y^2}}{dt} = v'^2 \int_0^t R_L(\tau) d\tau, \quad (6)$$

and
$$R_L(\tau) = \frac{1}{2v'^2} \left[\frac{d^2 \overline{Y^2}}{dt^2} \right]_{t \rightarrow \tau}. \quad (7)$$

Furthermore, substituting the empirical equation

$$R_L(\tau) = \exp -\frac{\tau}{\mathcal{F}_L}, \quad (8)$$

where \mathcal{F}_L is the integral timescale, into (5) and (6), we obtain

$$\mathcal{D}_t(t) = v'^2 \mathcal{F}_L \left\{ 1 - \exp -\frac{t}{\mathcal{F}_L} \right\}, \quad (9)$$

and
$$\overline{Y^2}(t) = 2v'^2 \mathcal{F}_L^2 \left[\frac{t}{\mathcal{F}_L} - \left\{ 1 - \exp -\frac{t}{\mathcal{F}_L} \right\} \right]. \quad (10)$$

The relations, expressed in (9) and (10), indicate that the effect of turbulent diffusion is increased by a larger intensity or scale of turbulence.

2.3. Turbulent diffusion in a decaying energy field

In a flow field where the turbulent energy decay is not negligible, i.e. $v'(t) \neq v'(t-\tau)$, as is usually encountered in actual flows, the one-particle diffusion has been expressed in more complicated terms by Batchelor & Townsend (1956); they suggested that the diffusion in the decay field could be treated as a steady process within a finite time by introducing a new time variable η , instead of the real time t , defined by

$$d\eta = \frac{dt}{t_s(t)}, \quad (11)$$

where $t_s(t)$ is the inherent timescale in the turbulent field.

Assuming that the decay of turbulent energy obeys the power law

$$v'^2 = A(t_0 + t)^{-n}, \quad (12)$$

where A and n are constant for the observation time and t is the time elapsed from a virtual time origin, as illustrated in figure 1, and then combining (12) with (3) and (4), the following equations are derived (the derivation is described in the Appendix):

$$\mathcal{D}_t(t) = \frac{1}{2} \frac{d\overline{Y^2}}{dt} = v_0'^2 t_0^2 \xi^{2m-1} \int_0^\eta \exp(-m\eta') R_L(\eta') d\eta', \quad (13)$$

$$\overline{Y^2}(t) = 2v_0'^2 t_0^2 \int_0^\eta \exp(2m\eta') \int_0^{\eta'} \exp(-m\eta'') R_L(\eta'') d\eta'' d\eta', \quad (14)$$

$$\text{and} \quad R_L(\tau) = \frac{1}{2v_0'^2} \left[\xi^{1-m} \left\{ \xi \frac{d^2 \bar{Y}^2}{dt^2} + \frac{1-2m}{t} \frac{d \bar{Y}^2}{dt} \right\} \right]_{t=\tau}, \quad (15a)$$

$$\text{where} \quad v_0' = v'(0), \quad m = 1 - \frac{1}{2}n, \quad \xi = 1 + \frac{t}{t_0}, \quad \eta = \ln \xi. \quad (15b)$$

Further, on the assumption that the distribution of R_L can be expressed as a steady exponential function for the η -region,

$$R_L(\eta) = \exp -\frac{\eta}{T_\eta}, \quad (16)$$

integrating (13) and (14), we obtain the relations

$$\mathcal{D}_t(t) = \frac{v_0'^2 t_0}{C_1} \xi^{2m-1} (1 - \xi^{-C_1}), \quad (17)$$

$$\text{and} \quad \bar{Y}^2(t) = \frac{2v_0'^2 t_0^2}{C_1} \left\{ \frac{1}{2m} (\xi^{2m} - 1) - \frac{1}{C_2} (\xi^{C_2} - 1) \right\}, \quad (18a)$$

where

$$\xi = 1 + \frac{t}{t_0}, \quad m = 1 - \frac{1}{2}n, \quad C_1 = m + \frac{1}{T_\eta}, \quad C_2 = m - \frac{1}{T_\eta}, \quad \frac{1}{T_\eta} = \frac{t_0}{\mathcal{F}_{L0}} + 1. \quad (18b)$$

Using the dimensionless quantities

$$t^* = \frac{t}{\mathcal{F}_{L0}}, \quad \mathcal{D}_t^* = \frac{\mathcal{D}_t}{\mathcal{D}_{t0}}, \quad Y^* = \frac{(\bar{Y}^2)^{\frac{1}{2}}}{A_{L0}}, \quad \mathcal{D}_{t0} = v_0' A_{L0}, \quad A_{L0} = v_0' \mathcal{F}_{L0}, \quad (19)$$

(17) and (18a) are rewritten as

$$\mathcal{D}_t^* = \frac{1}{C_1 I_\beta} (1 + I_\beta t^*)^{2m-1} \{1 - (1 + I_\beta t^*)^{-C_1}\}, \quad (20)$$

$$\text{and} \quad Y^{*2} = \frac{1}{C_1 I_\beta^2} \left[\frac{1}{2m} \{(1 + I_\beta t^*)^{2m} - 1\} - \frac{1}{C_2} \{(1 + I_\beta t^*)^{C_2} - 1\} \right], \quad (21a)$$

where

$$m = 1 - \frac{1}{2}n, \quad I_\beta = \frac{\mathcal{F}_{L0}}{t_0} = \frac{T_\eta}{1 - T_\eta}, \quad (T_\eta < 1), \quad C_1 = m + 1 + \frac{1}{I_\beta}, \quad C_1 + C_2 = 2m. \quad (21b)$$

Further, the following approximations are easily derived from (20) and (21a):

$$\mathcal{D}_t^* \doteq t^*; \quad Y^* \doteq t^*, \quad \text{for } t^* \rightarrow 0, \quad (22)$$

$$\mathcal{D}_t^* \propto t^{*2m-1}; \quad Y^* \propto t^{*m}, \quad \text{for } t^* \rightarrow \infty, \quad m \leq \frac{1}{2}. \quad (23)$$

3. Experimental

3.1. Experimental apparatus and procedure

The optical tracer-particle tracking method used for our Lagrangian measurements is fundamentally as follows.

(i) The Lagrangian behaviour of individual tracer particles suspended in a turbulent fluid flow can be detected as a particle image by a photodetector through the use of some optics.

(ii) Data on the position of the tracer particle at each moment, expressed in the

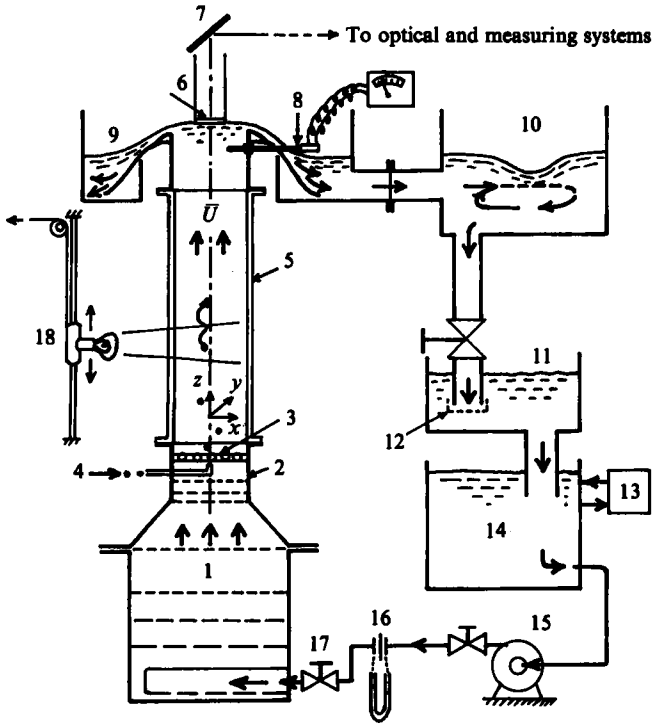


FIGURE 2. Schematic diagram of the experimental apparatus. 1, 2 calming section; 3 turbulence-generating grid; 4 tracer-particle inlet; 5 test section; 6 window pane; 7 mirror; 8 electromagnetic velocimeter; 9 overflow tank; 10, 11 bubble eliminating tank; 12 particle collector; 13 filter; 14 main tank; 15 pump; 16 flow meter; 17 flow-rate control valve; 18 flat lamp.

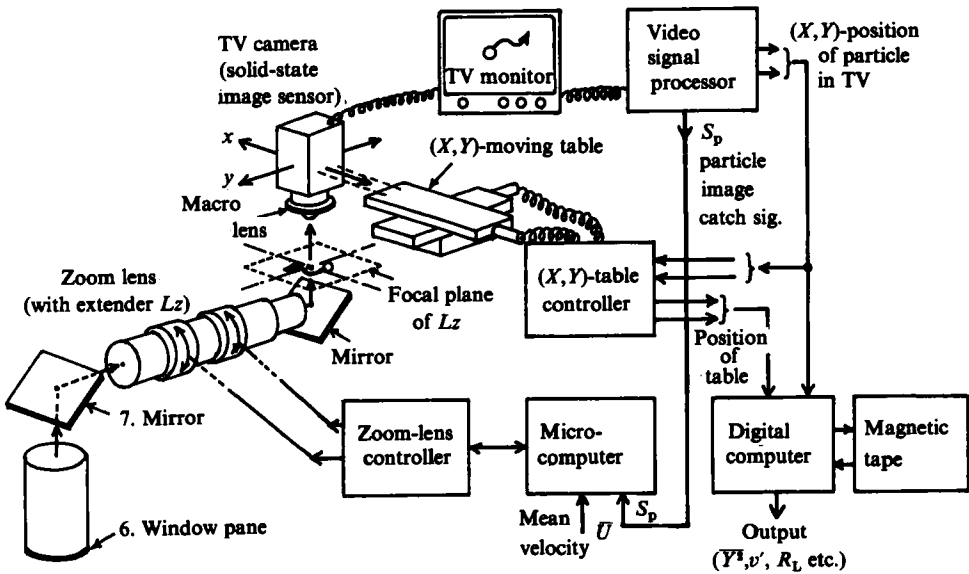


FIGURE 3. Schematic diagram of the optical and measuring systems.

Run no.	(a)						(b)						Symbols in figures
	M (cm)	M/d	Re_M	\bar{U} (cm/s)	Z_0/M	Re_λ	v'/\bar{U} (%)	λ_f (cm)	A_f (cm)	\mathcal{J}_L (s)			
1	0.76	5.2	1500	20.0	66	25	3.8	0.47	0.85	0.72	\triangle		
2	2.0	2.0	3900	19.5	20	40	5.6	0.51	1.21	0.60	\bullet		
3	2.0	2.0	5200	26.0	16	46	6.0	0.42	1.07	0.34	\odot		
4	2.0	2.0	6600	33.0	20	48	5.1	0.41	1.08	0.35	\circ		
5	4.0	4.0	8000	20.0	10	55	7.3	0.53	1.55	0.39	\blacksquare		
6	4.0	4.0	14000	35.0	10	66	6.4	0.40	1.34	0.22	\square		

TABLE 1. Experimental conditions and characteristics of turbulence. Turbulence-generating grid: bi-plane, square-mesh grid, runs 1-4 round rod, runs 5, 6 square rod

space coordinates, are continuously stored in a sub-memory, such as a magnetic-tape recorder, controlled by a mini-computer.

(iii) After appropriate processing of the data and calculations, information on the Lagrangian characteristics of the turbulent field is obtained in the form of numerical values and graphic curves.

For turbulent fluctuating fluid motion, the tracer particle must be chosen to be sufficiently small, i.e. less than the lengthscale of turbulence, and to be of density almost equal to that of the fluid, that it does not affect the turbulence structure and can follow the rapid fluctuation of the fluid. The following conditions for the tracer particle were required on the assumption that the mean velocity is of the order of 10 cm/s, the intensity of turbulence within 10%, the integral scale of eddy 10 mm or more, etc: (i) the tracer-particle is responsive to a frequency of about 20 Hz (Hinze 1972); (ii) its sedimentation or ascending speed in the water flow is less than 1 mm/s; (iii) its diameter is preferably roughly equal to or less than the Kolmogorov scale (at most 1 mm), but could be less than the Taylor's microscale (several mm), and (iv) the reflected light from the surface of the particle is as bright as possible. To satisfy these conditions as far as possible, a 'polystyrene ball' containing a little gas, of diameter 0.3–0.5 mm and of density 1.00 ± 0.02 , was prepared and used as the tracer particle in the measurements.

Figure 2 shows a schematic of the experimental apparatus, which has a test section of inner diameter 31 cm and length 100 cm, made of transport acrylic resin with an effective measurable dimension of about $15 \times 15 \text{ cm}^2 \times 70 \text{ cm}$. The experiment was conducted in a water flow with a mean velocity up to $\bar{U} = 40 \text{ cm/s}$, a flow rate of $1.8 \text{ m}^3/\text{min}$ and Reynolds number, $Re_D = 1.24 \times 10^5$. In the approximately homogeneous isotropic turbulent field downstream of a turbulence-generating grid (of bi-plane, square-mesh type, with mesh length $M = 2.0$ or 0.76 cm , and round or square rods of diameter $d = 1.0$ or 0.146 cm), the Lagrangian behaviour of individual tracer particles, excluding buoyancy effects, in the perpendicular (x, y)-plane to the main flow direction (z), could be measured by a television camera with a solid-state image sensor (element number: 320×244) through a window pane, a zoom lens, etc. (see figure 3).

To obtain a reliable Lagrangian correlation coefficient R_L , the spatial resolution of the measurements had to be sufficiently high (about $50 \mu\text{m}$ in the real measurement space) that the Lagrangian fluctuation velocity could be exactly detected at every moment (actually every $\frac{1}{60} \text{ s}$). This was achieved by controlling the zoom lens with a microcomputer and by tracking the television camera in accordance with particle motions using an (X, Y)-moving table. Thus, $R_L(\tau)$ could be directly obtained from the definition equation (2) rather than from the second derivatives of \bar{Y}^2 . In previous studies $R_L(\tau)$ has been obtained from (7), namely the second derivatives of \bar{Y}^2 , with the assumption that the turbulent field was homogeneous isotropic and with negligible decay in intensity. Therefore, little exact data on $R_L(\tau)$ has been available, particularly for the decaying turbulent energy field. The present values of $R_L(\tau)$ obtained directly from the correlation between Lagrangian fluctuations are fairly accurate and also have taken account of the turbulent-energy decay.

Some Lagrangian data measured under the experimental conditions listed in table 1 (a) will be presented in the next section.

3.2. Measured data

The experimental conditions and some characteristics of the turbulence are summarized in table 1 (b). The turbulent Reynolds number $Re_\lambda = u'\lambda_g/\nu$ (λ_g is the lateral

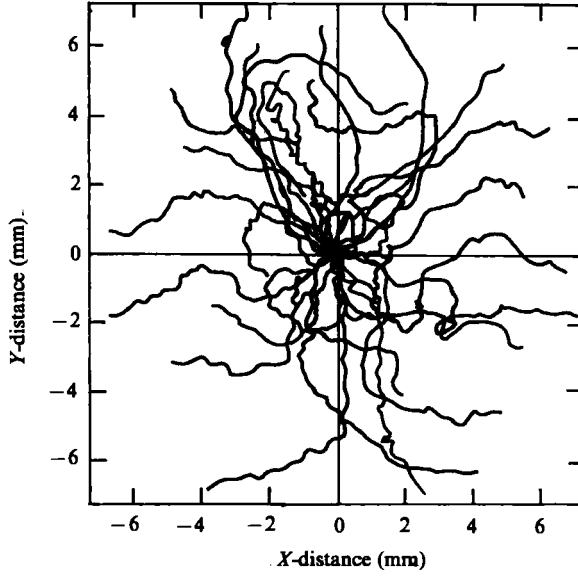


FIGURE 4. Particle trajectories in the (x, y) -plane. Starting point $(0, 0)$; Data number 25; $\bar{U} = 26$ cm/s; $Z_0 = 30$ cm downstream of a grid.

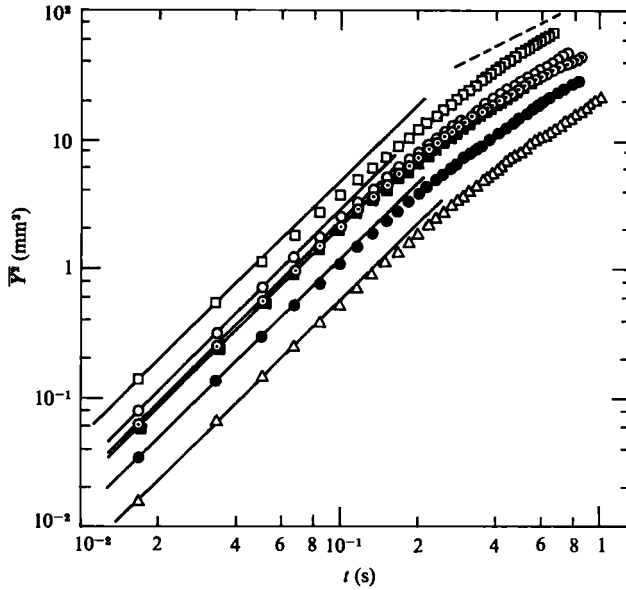


FIGURE 5. Lateral particle diffusion from a fixed point in a grid turbulence. See table 1 for the symbols and the experimental conditions. —, $\bar{Y}^2 = v'^2 t^2$; ---, $\bar{Y}^2 \propto t$.

Taylor's microscale and ν the kinematic viscosity of fluid) was restricted in our experiments to the moderate or low range of $20 \lesssim Re_\lambda \lesssim 70$ because of the capability limits of the flow and measuring systems. A_f in table 1(b), the Eulerian longitudinal integral scale of $f(r)$, was determined from the empirical equation for the Eulerian measurement (Sato, Yamamoto & Mizushima 1983), as well as the longitudinal double velocity correlation coefficient $f(r)$ for the spatial distance r .

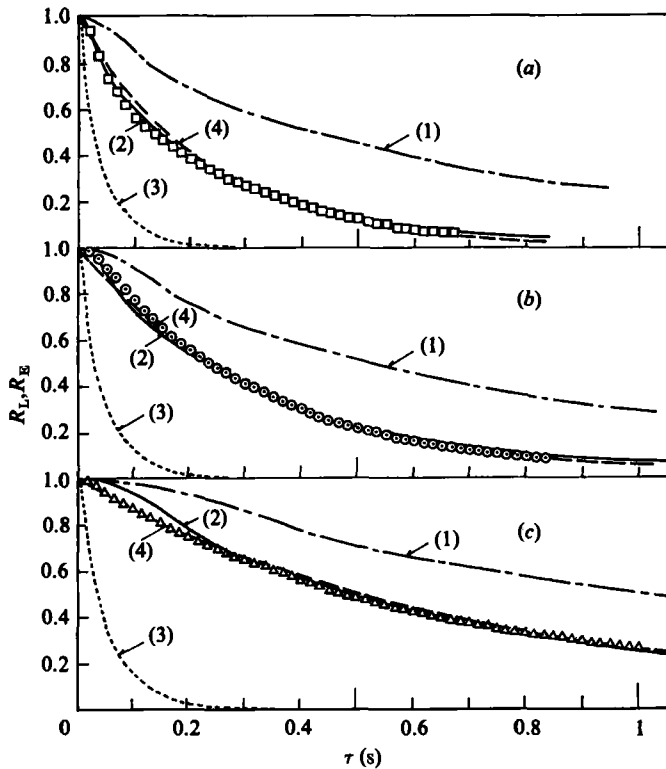


FIGURE 6. Distribution of the Lagrangian velocity autocorrelation coefficient in grid turbulence. (a) The turbulent Reynolds number $Re_\lambda = 66$; (b) 46; (c) 25. Measurements: $\square \odot \triangle$, see table 1. Calculations: (1) — — —, $R_E(\tau = r/v')$; (2) — — —, $R_E(\tau = \beta r/v')$; (3) ·····, $E_E(\tau = r/\bar{U})$; (4) - - - - - , $R_L(\tau) = \exp(-\tau/\mathcal{T}_L)$.

Figures 4, 5 and 6 were prepared from the raw measured data. Figure 4 shows the trajectory of particles in the (x, y) -plane perpendicular to the main flow direction (z) . Figure 5 shows the variation of lateral particle diffusion $\overline{Y^2}$ due to the turbulent fluctuation with time elapsed, on a logarithmic scale. It can be seen from the figure that for short times Y increases asymptotically along the solid straight line

$$\overline{Y^2} = v_0'^2 t^2, \quad (24)$$

and for longer times it tends to deviate down from the line gradually. In figure 6, the measured values of $R_L(\tau)$ are plotted against the lag time τ , and compared with various calculated curves, which will be discussed in the next section.

4. Results and discussion

4.1. Comparison with Eulerian measurements

In figure 6 the distributions of the Eulerian autocorrelation coefficient R_E are shown together with the Lagrangian data for R_L . These values of R_E were calculated from the Eulerian spatial double correlation coefficient $f(\tau)$ based on the empirical equation proposed by Sato *et al.* (1983); curves (1), (3) and (2) represent $R_E(\tau)$ for the time lags $\tau = r/v'$, $\tau = r/\bar{U}$ and $\tau = \beta r/v'$ (where β is constant) respectively. The value of β will be given below. As is clear from figure 6, the distribution of measured $R_L(\tau)$

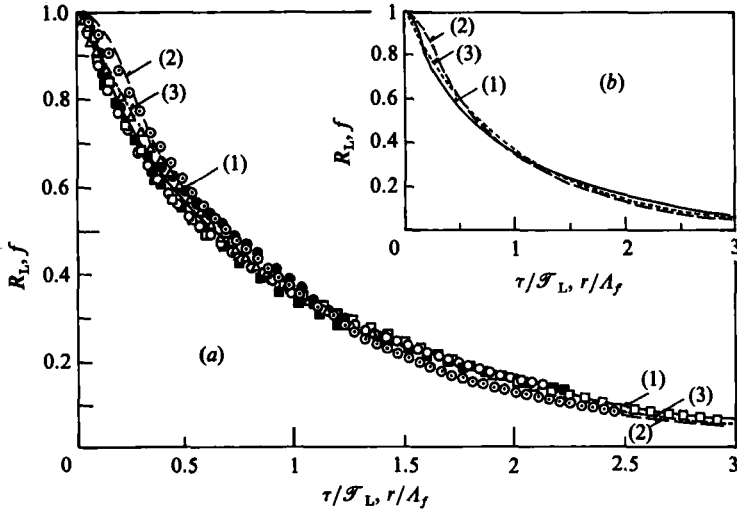


FIGURE 7. Distribution of the Lagrangian autocorrelation coefficient normalized with the integral scale. (a) Measurement: $R_L(\tau/\mathcal{T}_L)$, see table 1 for the symbols. (b) Calculation: (1) —, $f(r/A_f)$ for $Re_\lambda = 70$; (2) - - - -, $f(r/A_f)$ for $Re_\lambda = 25$; (3) ·····, $R_L(\tau/\mathcal{T}_L) = \exp(-\tau/\mathcal{T}_L)$.

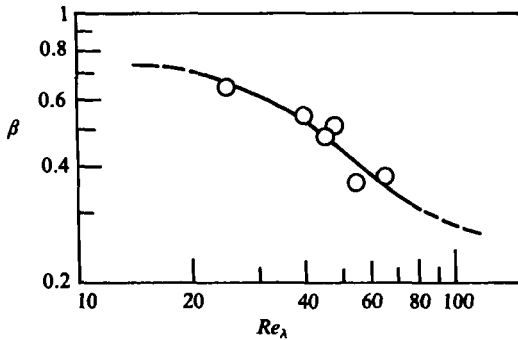


FIGURE 8. Ratio of Lagrangian to Eulerian integral lengthscales against the turbulent Reynolds numbers.

decreases fast compared with that of $R_E(\tau = r/v')$ represented by curve (1), for any of the experimental conditions (a), (b) or (c). This fact has been proved by many investigators (e.g. Corrsin 1959, 1963; Saffman 1962; Snyder & Lumley 1971; Shlien & Corrsin 1974; Hinze 1975).

Figure 7 shows the distribution of measured R_L against the time lag normalized with the integral scale \mathcal{T}_L , compared with that of the Eulerian $f(r)$ against r/A_f and the empirical exponential equation (8). Broadly, good agreement between these distributions was obtained except for the range of small τ or r , τ/\mathcal{T}_L or $r/A_f < 0.5$. However, for the analysis of the turbulent diffusion process, the integral value of $R_L(\tau)$ is important, as can be seen from (3), and so the detailed behaviour of $R_L(\tau)$ and its fine structure, for the short lag time in particular, is not required.

For the integral lengthscale of turbulence, then, the ratio of Lagrangian to Eulerian values is commonly used, as defined by

$$\beta = \frac{A_L}{A_f} = \frac{v' \mathcal{T}_L}{A_f}. \tag{25}$$

In figure 8 the values of β obtained by the present measurements are plotted against the turbulent Reynolds numbers Re_λ . The decaying field for grid turbulence, $10 \lesssim Z_0/M \lesssim 20$, downstream of the grid, was regarded as an initial decay period (e.g. see Comte-Bellot & Corrsin 1966; Sato & Yamamoto 1984). Therefore, the values of β are only dependent upon Re_λ under the present experimental conditions. It was found from figure 8 that, for the range of $20 \lesssim Re_\lambda \lesssim 70$, β was within the values of 0.6 to 0.3, becoming lower as Re_λ increased, although this has still to be confirmed for a wider range of Re_λ . This tendency of β to vary with Re_λ agrees with the opinion of Hinze (1975) and the values are reasonably close to the calculations presented by Corrsin (1959), Saffman (1962), etc. and the experimental data of Snyder & Lumley (1971), etc.

The determination of β enables us to predict the distribution of the Lagrangian correlation R_L using the Eulerian R_E . In figure 6, the curves of $R_E(\tau)$ against the compressed lag time $\tau = \beta r/v'$ have been drawn as solid lines, along with the measured $R_L(\tau)$. The calculated values of $R_E(\tau = \beta r/v')$ agree so well with the experimental value of $R_L(\tau)$ that we could not on the whole distinguish the curves from the measured R_L .

Incidentally, it should be noted that the correlation coefficient $R_E(\tau)$ for $\tau = r/v'$ is considered in the Eulerian frame moving with the mean flow, and so is different from the Eulerian autocorrelation coefficient $R_E(\tau')$ measured at any fixed point with a lag time τ' corresponding to r/\bar{U} in the uniform flow of mean velocity \bar{U} . $R_E(\tau')$ decreases rather faster than $R_L(\tau)$, as the dotted line in figure 8 indicates. If \mathcal{T}_E is the Eulerian integral timescale,

$$\mathcal{T}_E = \int_0^\infty R_E(\tau') d\tau' = \frac{1}{\bar{U}} \int_0^\infty f(r) dr = \frac{A_f}{\bar{U}}, \quad (26)$$

the ratio β' of the Lagrangian and Eulerian integral timescales,

$$\beta' = \frac{\mathcal{T}_L}{\mathcal{T}_E} = \beta \left(\frac{\bar{U}}{u'} \right), \quad (27)$$

is higher in value than β . Substituting $\beta = 0.6 - 0.3$ and $u'/\bar{U} = 0.05 - 0.1$ into (27), we obtain $\beta' = 12 - 3$. This indicates that in the laboratory frame with the mean velocity \bar{U} , the Eulerian is obviously less than the Lagrangian, as pointed out by Saffman (1962).

Figure 9 shows a comparison of the Lagrangian and Eulerian turbulent energy spectra for the frequency (n_f) region. Here, the Lagrangian spectrum $E_{L1}(n_f)$ and the Eulerian one-dimensional energy spectrum $E_{E1}(n_f)$ were obtained from the Fourier transformations

$$E_{L1}(n_f) = 4 \int_0^\infty R_L(\tau) \cos 2\pi n_f \tau d\tau, \quad (28)$$

$$E_{E1}(n_f) = \frac{4}{\bar{U}} \int_0^\infty f(r) \cos \frac{2\pi n_f r}{\bar{U}} dr, \quad (29)$$

by using the correlation coefficients $R_L(\tau)$ and $f(r)$ respectively. The Lagrangian spectra apparently consisted of lower-frequency components compared with the Eulerian ones. This also demonstrates that larger-scale motion contributes more effectively to the turbulent diffusion.

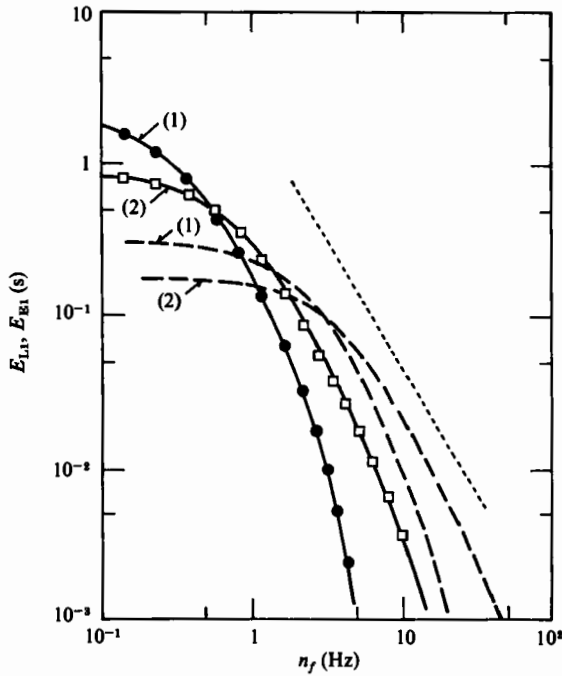


FIGURE 9. Comparison of Lagrangian and Eulerian energy spectra in isotropic turbulence. —, Lagrangian measurement; ---, Eulerian measurement; ·····, slope of $-\frac{5}{3}$ power law. (1) ●, $Re_\lambda = 40$, $\bar{U} = 19.5$ cm/s, $v'/\bar{U} = 5.6\%$; (2) □, $Re_\lambda = 66$, $U = 35.0$ cm/s, $v'/\bar{U} = 6.4\%$.

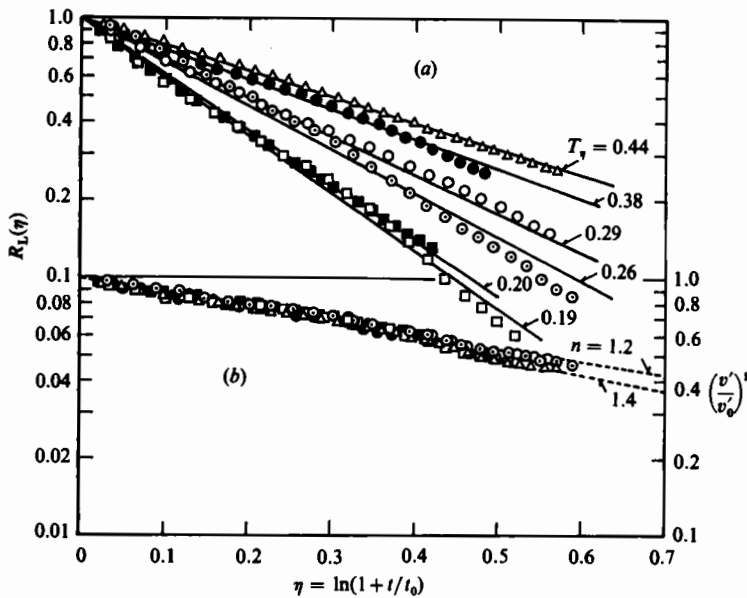


FIGURE 10. Distribution of R_L and $(v'/v_0')^2$ against η . (a) $R_L(\eta)$: —, $\exp(-\eta/T_\gamma)$, for: Δ , $T_\gamma = 0.44$; ●, 0.38; ○, 0.29; ⊙, 0.26; ■, 0.20; □, 0.19. (b) $(v'/v_0')^2$: ·····, $\exp(-n\eta)$, for $n = 1.2$ and 1.4. See table 1 for the symbols.

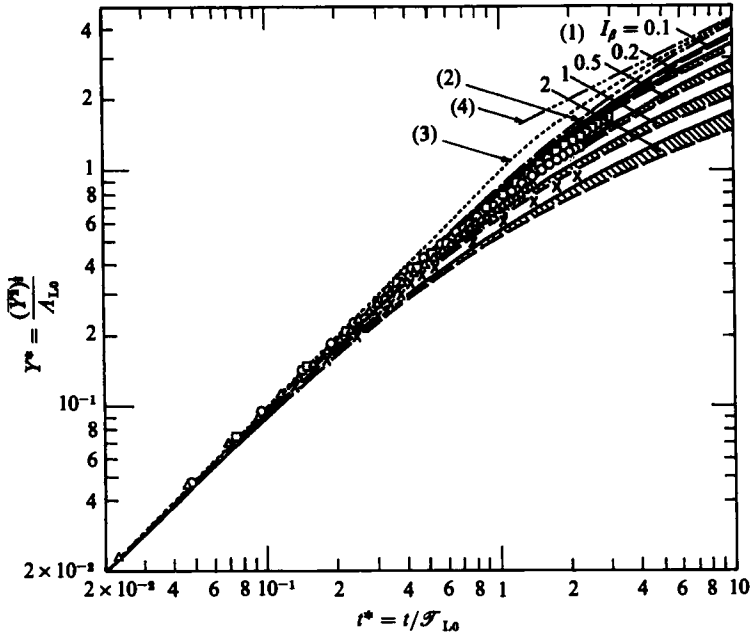


FIGURE 11. Lateral particle diffusion from a fixed source in a decaying turbulent field. Measured data: present work, \square , $Re_\lambda = 66$, $n = 1.2$, $I_\beta = 0.25$; \circ , $Re_\lambda = 48$, $n = 1.25$, $I_\beta = 0.41$; \triangle , $Re_\lambda = 25$, $n = 1.3$, $I_\beta = 0.79$; Shlien & Corrsin (1974), \times , $Re_\lambda = 70$, $n = 1.25$, $I_\beta = 1.3$. Calculated curves: (1) (shaded) equation (21) with $n = 1.2$ (—) and 1.4 (---); (2) —·—, equation (10); (3) ·····, equation (31); (4) —·—·—, $Y^* = (2t^*)^{1/2}$.

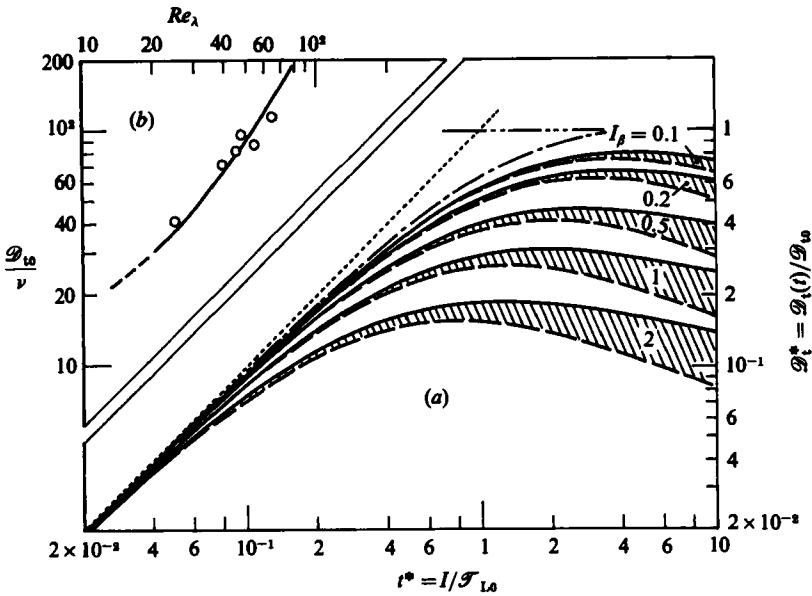


FIGURE 12. Lateral diffusion coefficient in a decaying turbulent field. (a) \mathcal{D}_t^* vs. t^* , the shaded lines, equation (20) with $n = 1.2$ (—) and 1.4 (---); —·—, equation (9); ·····, $\mathcal{D}_t^* = t^*$; —·—·—, $\mathcal{D}_t^* = 1$. (b) \mathcal{D}_{t0}/ν vs. Re_λ .

4.2. Turbulent diffusion in the decaying field

In a field of decaying turbulent intensity, the diffusion of fluid particles from a fixed point source is represented by \mathcal{D}_t or $\overline{Y^2}$ as in (17) and (18a), or the dimensionless equations (20) and (21a). To apply these diffusion equations, the assumptions of (16) and (12) have to be experimentally verified. This is done in figure 10, where in figure 10(a) the distribution of R_L , and in figure 10(b) the variation of the decay of turbulent intensity, are plotted against the newly defined time variable η as semi-logarithmic graphs. The results in figure 10(a) for the measured R_L and (16) with various T_η , drawn by solid lines, agree well with each other and so verify (16). Further, it can be seen from figure 10(b) that the decay law of (12) with the exponent n of about 1.2–1.4 holds for the observed flow field (the distance of up to about 70 cm downstream of the grid in the present set-up) where we could regard it as the initial decay stage, since (12) can be transformed to

$$\left(\frac{v'}{v_0}\right)^2 = \exp(-n\eta). \quad (30)$$

Figure 11 shows the dimensionless variation of the lateral particle diffusion for the time elapsed, defined by (19), to compare the measured data with some calculated curves on log-log scales. The measured data agree better with (21a) containing the parameters n and I_β , indicated by bold solid and broken lines in figure 11, than with the other calculated curves such as (10) for negligible decay (chain line), the simple equation for a step function of R_L and for $n = 0$,

$$\overline{Y^2}(t) = \begin{cases} v'^2 t^2, & \text{for } t \leq \mathcal{T}_L, \\ v'^2 \mathcal{T}_L^2 \frac{2t}{\mathcal{T}_L} - 1, & \text{for } t > \mathcal{T}_L, \end{cases} \quad (31)$$

and their asymptotical equation for long time, $Y^* = (2t^*)^{\frac{1}{2}}$. These results indicate that for a comparatively short time, $t^* < 1$, the diffusion width Y^* grows as (10), without the decay effect, nearly proportionally to the time, but for longer times, $t^* > 1$, it deviates by a small amount from the equation in accordance with the extent of the decay.

Figure 12 shows the lateral turbulent diffusion coefficient \mathcal{D}_t in the decaying field. In figure 12(a) the effect of the energy decay on the diffusion coefficient is shown by comparing dimensionless curves against the elapsed time calculated from (20) with $n = 1.2$ or 1.4 for several values of the parameter I_β , with the non-decay equation (9) (a dot-dash line) and its asymptotical lines; $\mathcal{D}_t^* = t^*$, for $t^* \rightarrow 0$ and $\mathcal{D}_t^* = 1$, for $t^* \rightarrow \infty$. As with Y^* in figure 11, it is found that \mathcal{D}_t^* is almost proportional to t^* at first but for longer times is reduced by the effect of turbulent energy decay as values of n and I_β increase. In figure 12(b), the ratio of the measured data of $\mathcal{D}_{t_0} = v'_0 A_{L0}$ to the molecular kinematic viscosity ν are plotted against the turbulent Reynolds numbers Re_λ . Apparently, the turbulent diffusion coefficient \mathcal{D}_{t_0}/ν becomes larger with the increase of Re_λ ; it shows a reasonable value of about 30–100 times β of 20–70.

5. Conclusions

Exact measured data for turbulent diffusion and Lagrangian velocity autocorrelation were obtained in approximately homogeneous isotropic grid turbulence using a newly developed optical tracer-particle tracking method. Comparing the experi-

mental data on the Lagrangian characteristics with theoretical analysis yielded the following remarkable results.

(i) The turbulent intensity v' and the integral scale corresponding to the mixing length A_L contribute effectively to the mixing and diffusion mechanisms of turbulence.

(ii) The distributions of Lagrangian and Eulerian autocorrelation coefficients become fairly similar to each other after modification of then time axis with β , which represents the ratio of Lagrangian to Eulerian integral lengthscales.

(iii) The ratio β is approximately 0.6 to 0.3 for the turbulent Reynolds-number range of $Re_\lambda = 20-70$, becoming lower as Re_λ increases.

(iv) For a short release time the lateral particle diffusion $(\overline{Y^2})^{\frac{1}{2}}$ is roughly proportional to the time t almost independently of the turbulent energy decay.

(v) For a time longer than the integral timescale \mathcal{T}_L , the turbulent energy decay exerts more influence on the diffusion process to weaken the growth of $\overline{Y^2}$.

We also offer some comments on how random motion by the random field itself affects the timescales; specifically, whether the Lagrangian timescale is greater or less than the Eulerian timescale. The experimental results presented here corroborated that the Lagrangian integral timescale \mathcal{T}_L is less than the equivalent Eulerian timescale $\mathcal{T}_E (= A_f/u')$ in the frame relative to which the mean velocity is regarded as zero. This is consequently consistent with the previous theoretical approaches such as the independence approximation (Corrsin 1959; Saffman 1962; Weinstock 1976) and the computer simulation by Kraichnan (1970). In the laboratory frame with mean velocity \overline{U} , it was of course obvious that the Lagrangian scale \mathcal{T}_L is several or more times greater than the Eulerian one \mathcal{T}_E , as expressed in (27).

This work was partially supported by a Grant in Aid for Scientific Research (No. 58101009) from the Ministry of Education, Science and Culture of Japan.

Appendix. Derivation of the diffusion equation in a decaying turbulent field

A.1. Relationship between a new variable η and real time t

Batchelor & Townsend (1956) have suggested that even for a decaying turbulent field, the diffusion process of fluid particles could be treated as a steady approximation, by introducing a new time variable η defined by (11).

The intrinsic timescale t_s in (11) would be considered to be only dependent upon the characteristic lengthscale $A(t)$ and the fluctuation velocity $v'(t)$ in the turbulent field;

$$t_s(t) = \frac{A(t)}{b'(t)}. \quad (\text{A } 1)$$

The relation of the longitudinal integral lengthscale A_f and the fluctuation velocity u' , obtained by the Eulerian measurements, can be predicted exactly as has been done by many previous investigations (e.g. Monin & Yaglom 1971). Then, assuming the empirical relations

$$v' \doteq u'; \quad A \doteq \beta A_f, \quad \beta \doteq \text{const.}, \quad (\text{A } 2)$$

and using the relation between A_f and u' , we can determine the function form of $t_s(t)$ as follows: Assuming that the decay of the turbulent energy u' obeys the power law,

$$u'^2(t) = A(t_0 + t)^{-n}, \quad A = \text{const.}, \quad (\text{A } 3)$$

the longitudinal microscale for isotropic turbulence λ_f is given by

$$\lambda_f^2 = \frac{20\nu u'^2}{-(du'^2/dt)} = \frac{20\nu(t_0+t)}{n}. \quad (\text{A } 4)$$

Further, the following approximation has been proposed by Sato *et al.* (1983) to relate A_f and λ_f :

$$\frac{A_f}{\lambda_f} = \frac{0.05Re_\lambda \propto u' \lambda_f}{\nu}. \quad (\text{A } 5)$$

Combination of (A 2), (A 4) and (A 5) with (A 1) yields

$$t_s(t) = \frac{t_0+t}{C}, \quad C = \text{const.} \quad (\text{A } 6)$$

Then, integrating (11) by use of (A 6), we obtain

$$\eta = \int_0^t \frac{dt}{t_s(t)} = C \ln \left(1 + \frac{t}{t_0} \right). \quad (\text{A } 7)$$

Further, replacing η/C by η in equation (A 7), we then obtain

$$\exp \eta = 1 + \frac{t}{t_0}; \quad dt = t_0 \exp \eta d\eta. \quad (\text{A } 8)$$

A.2. Velocity autocorrelation and turbulent diffusion

Assuming that the function $R_L(\eta - \eta')$ is homogeneous stationary, and using (3) and (4), we can determine the function form of $\overline{Y^2}(t)$ and $\mathcal{D}_t(t)$ as follows: By using the decay equation of turbulent intensity rewritten from (28),

$$v'(t) = v'_0 \exp(\frac{1}{2}n\eta), \quad v'_0 = v'(0),$$

the definition of

$$\eta' = \ln \left\{ 1 + \frac{t-\tau}{t_0} \right\},$$

and (A 8), and integrating the right-hand side of (4), we obtain

$$\frac{1}{2} \frac{d\overline{Y^2}}{dt} = v'_0{}^2 t_0 \exp(-\frac{1}{2}n\eta) \int_0^\eta \exp\{-(1-\frac{1}{2}n)\eta'\} R_L(\eta-\eta') d\eta'. \quad (\text{A } 9)$$

Here, the application of the convolution integral formula

$$\int_0^t f_1(s)f_2(t-s) ds = \int_0^t f_1(t-s)f_2(s) ds,$$

to (A 9) yields

$$\frac{1}{2} \frac{d\overline{Y^2}}{dt} = v'_0{}^2 t_0 \exp\{(2m-1)\eta\} \int_0^\eta \exp(-m\eta') R_L(\eta') d\eta'. \quad (\text{A } 10)$$

Rewriting equation (A 10) with the aid of equation (A 8), we obtain (13) in §2. Further, the integration of (A 10) with respect to time t leads to (14) for $\overline{Y^2}(t)$.

In addition, (15) is derived from the differentiation of (A 10) or (14) with respect to t .

REFERENCES

- BATCHELOR, G. K. & TOWNSEND, A. A. 1956 In *Surveys in Mechanics* (ed. G. K. Batchelor & R. M. Davies), p. 352. Cambridge University Press.
- COMTE-BELLOT, G. & CORRSIN, S. 1966 *J. Fluid Mech.* **25**, 657.
- CORNELIUS, K. C. & FOSS, J. F. 1978 *Special Report to SQUID*, no. 8960-11, Michigan State University.
- CORRSIN, S. 1959 *Adv. Geophys.* **6**, 161.
- CORRSIN, S. 1963 *J. Atmos. Sci.* **20**, 115.
- HINZE, J. O. 1972 *Prog. Heat Mass Transfer* **6**, 433.
- HINZE, J. O. 1975 *Turbulence*, 2nd edn, chap. 5. McGraw-Hill.
- KRAICHNAN, R. H. 1970 *Phys. Fluids* **13**, 22.
- MONIN, A. S. & YAGLOM, A. M. 1971 *Statistical Fluid Mechanics* (ed. J. L. Lumley), vol. 1, chap. 5. M.I.T. Press.
- SAFFMAN, P. G. 1962 *Appl. Sci. Res.* **11A**, 245.
- SATO, Y., YAMAMOTO, K. & MIZUSHINA, T. 1983 *J. Chem. Engng Japan* **16**, 273.
- SATO, Y. & YAMAMOTO, K. 1984 *AIChE J.* **30**, 831.
- SHLIEN, D. J. & CORRSIN, S. 1974 *J. Fluid Mech.* **62**, 255.
- SNYDER, W. H. & LUMLEY, J. L. 1971 *J. Fluid Mech.* **48**, 41.
- TAYLOR, G. I. 1921 *Proc. Lond. Math. Soc.* **20**, 196.
- WEINSTOCK, J. 1976 *Phys. Fluids* **11**, 1702.